phoretically labeled cells are mature (innervated) receptor cells. Furthermore, the incidence of bitter-responsive dye-labeled cells (18%) is remarkably close to the incidence of cells expressing candidate bitter receptors [15 to 20% (*1*)], suggesting that dye-labeled cells are representative taste receptor cells.
11. Ca^{2+} signals presumably indicate physiological activation and presage neurotransmitter release. However, the absence of Ca^{2+} signals does not necessarily indicate that the cell has not been affected (for example, if a stimulus inhibits the taste cell).
12. C. P. Richter, K. H. Clisby, *Am. J. Physiol.* **134**, 157 (1941).
13. H. D. Patton, T. C. Ruch, *J. Comp. Psychol.* **37**, 35 (1944).
14. S. D. Koh, P. Teitelbaum, *J. Comp. Physiol. Psychol.* **54**, 223 (1961).
15. E. Tobach, J. S. Bellin, D. K. Das, *Behav. Genet.* **4**, 405 (1974).
16. K. Iwasaki, M. Sato, *Chem. Senses* **6**, 119 (1981).
17. J. I. Glendinning, *Physiol. Behav.* **56**, 1217 (1994).
18. A. K. Thaw, *Chem. Senses* **21**, 189 (1996).
19. N. K. Dess, *Physiol. Behav.* **69**, 247 (2000).
20. Bath application of cycloheximide (0.1 to 300 μM), denatonium benzoate (3 to 3000 μM), quinine HCl (10 to 3000 μM), SOA (10 to 1000 μM), and PTC (10 to 1000 μM) induced transient Ca^{2+} responses in taste cells in 83% of foliate taste buds tested (43 out of 52 taste buds). At the concentrations used, none of the compounds interfered with fluorescence intensity.
21. Lowering extracellular Ca^{2+} appeared to increase intracellular Ca^{2+} transiently in many cells (Fig. 2D), consistent with previous findings in catfish taste cells [M. M. Zviman, D. Restrepo, J. H. Teeter, *J. Membr. Biol.* **149**, 81 (1996)].
22. Quinine- and denatonium-responsive taste cells (n = 2 for each) also did not show Ca^{2+} increases when depolarized by 50 mM KCl [see also (*25*)].
23. P. M. Hwang, A. Verma, D. S. Bredt, S. H. Snyder, *Proc. Natl. Acad. Sci. U.S.A.* **87**, 7395 (1990).
24. A. I. Spielman *et al.*, *Am. J. Physiol.* **270**, 926 (1996).
25. M. H. Akabas, J. Dodd, Q. Al-Awqati, *Science* **242**, 1047 (1988).
26. T. Ogura, A. Mackay-Sim, S. C. Kinnamon, *J. Neurosci.* **17**, 3580 (1997).
27. The response thresholds versus the behavioral thresholds, respectively, were as follows: 0.1 to 0.3 μM (Fig. 2F) versus 0.2 to 2 μM for cycloheximide (*15*); 10 to 30 μM (red circles, Fig. 3C) versus 8 to 20 μM for quinine (*13*, *14*, *17*, *18*); 3 to 10 μM (gray triangles, Fig. 3C) versus ~1 μM for denatonium (*16*, *17*); 100 to 300 μM (blue triangles, Fig. 3C) versus 20 to 600 μM for PTC (*12*, *15*); and 30 to 100 μM (green squares, Fig. 3C) versus 100 to 200 μM for SOA (*19*).
28. S. Bernhardt, M. Naim, U. Zehavi, B. Lindemann, *J. Physiol.* **490**, 325 (1996).
29. J. F. Delwiche, Z. Buletic, P. A. S. Breslin, paper presented at the XII International Symposium on Olfaction and Taste/XIV Biennial Congress of the European Chemoreception Research Organisation, Brighton, UK, 20 to 24 July 2000.
30. T. Leinders-Zufall, G. M. Shepherd, C. A. Greer, F. Zufall, *J. Neurosci.* **18**, 5630 (1998).
31. This work was supported by NIH grants DC00374 (S.D.R.) and DC04525-01 (A.C.) from the National Institute on Deafness and Other Communication Disorders.

17 October 2000; accepted 22 January 2001

Modulation of Oscillatory Neuronal Synchronization by Selective Visual Attention

Pascal Fries,[1]* John H. Reynolds,[1,2] Alan E. Rorie,[1] Robert Desimone[1]

In crowded visual scenes, attention is needed to select relevant stimuli. To study the underlying mechanisms, we recorded neurons in cortical area V4 while macaque monkeys attended to behaviorally relevant stimuli and ignored distracters. Neurons activated by the attended stimulus showed increased gamma-frequency (35 to 90 hertz) synchronization but reduced low-frequency (<17 hertz) synchronization compared with neurons at nearby V4 sites activated by distracters. Because postsynaptic integration times are short, these localized changes in synchronization may serve to amplify behaviorally relevant signals in the cortex.

Visual scenes typically contain multiple stimuli competing for control over behavior, and attention biases this competition in favor of the most relevant stimulus (*1*). Correspondingly, if two competing stimuli are contained within the receptive field (RF) of an extrastriate neuron, and one of them is attended, the neuron responds as though only the attended stimulus is present (*2*–*6*). Thus, inputs from attended stimuli must have an advantage over inputs from unattended stimuli (*6*). This is apparently not always achieved by a simple increase in firing rates to an attended stimulus, however, because firing rates to a single, high-contrast stimulus in the RF are often not increased with attention (*2*, *5*, *7*). As an alternative to increases in firing rate, one potential "amplifier" of selected neural signals is gamma-frequency synchronization (*8*–*17*). Small changes in gamma-frequency synchronization with attention might lead to pronounced firing-rate changes at subsequent stages (*10*, *18*). Indeed, it was recently reported that neurons in monkey somatosensory cortex showed stronger synchronization during a tactile task than during a visual task, which was presumably caused by increased attention to the tactile stimulus in the tactile task (*19*). However, it is not clear whether the enhanced synchronization was present throughout the somatosensory system or whether it was restricted to those neurons processing the relevant tactile stimuli. To be useful in selective visual attention, enhanced synchronization would need to be confined to neurons activated by the features of attended stimuli, sparing neurons activated by distracters.

We recorded both spikes from small clusters of neurons (multi-unit activity) and local field potentials (LFPs) simultaneously from multiple V4 sites with overlapping receptive fields (RFs) (*20*). The monkey fixated a central spot, and after a short delay, two stimuli were presented at equal eccentricity, one inside and one outside the RFs (Fig. 1C). On separate trials, the monkey's attention was directed to either stimulus location (*21*), and we compared neuronal activity between the two attention conditions. We refer to the condition with attention into the RF as "with attention," always implicitly comparing with identical sensory conditions but with attention outside the RF.

One example pair of recording sites is shown in Fig. 1. The response histograms (Fig. 1D) show stimulus-evoked responses but no clear effect of attention, either during the prestimulus delay or during the stimulus period. To examine the effect of attention on synchronization, we calculated spike-triggered averages (STAs) of the LFP (*11*, *14*, *22*). The STAs revealed oscillatory synchronization between spikes and LFP from two separate electrodes, both during the delay (Fig. 1, E and F) and the stimulus period (Fig. 1, H and I). During the delay, the power spectra of the STAs (Fig. 1G) were dominated by frequencies below 17 Hz. With attention, this low-frequency synchronization was reduced (*23*). During the stimulus period, there were two distinct bands in the power spectrum of the STAs (Fig. 1J), one below 10 Hz and another at 35 to 60 Hz. With attention, the reduction in low-frequency synchronization was maintained and, conversely, gamma-frequency synchronization was increased.

To determine whether these changes in synchronization were precisely localized within V4, we made additional recordings with the stimulus outside the RF very close to the RF border (Fig. 2). Even with closely spaced stimuli, we found the same attentional modulation of synchronization as with the second stimulus far away (Fig. 2, C to E). In

[1]Laboratory of Neuropsychology, National Institute of Mental Health, National Institutes of Health, Building 49, Room 1B80, 9000 Rockville Pike, Bethesda, MD 20892–4415, USA. [2]Systems Neurobiology Laboratory, The Salk Institute for Biological Studies, 10010 North Torrey Pines Road, La Jolla, CA 92037–1099, USA.

*To whom correspondence should be addressed. E-mail: fries@ln.nimh.nih.gov

addition to these changes in synchronization, firing rates to the RF stimulus were also moderately suppressed when attention was directed to the surround stimulus (Fig. 2B), consistent with previous studies of competitive interactions between stimuli in V4 RFs (*2*, *5*, *6*). Large firing-rate changes with attention occurred only with a competing stimulus very near to the RF border.

Across the set of recordings, attentional modulations of oscillatory synchronization were similar to the presented examples. We quantified the STA modulation by calculating the spike-field coherence (SFC) (*14*), which measures phase synchronization between spikes and LFP oscillations as a function of frequency. The SFC is normalized for spike rate and spectral power of the LFP and is therefore immune to changes in these parameters. The SFC ranges from 0 (complete lack of synchronization) to 1 (perfect phase synchronization). Computing the coherence between a point process (spikes) and an analog signal (LFP) is a special case, and therefore detailed information is given as supplementary material (*24*). We pooled data for the stimulus configurations in which the distracters were near to and far from the RF.

For the delay period (Fig. 3, A and B), low-frequency SFC was reduced by a median of 51% with attention (160 decreases, 23 increases; $P < 10^{-6}$) (*25*). The delay-period STAs did not show clear gamma-frequency modulations (Fig. 1, E to G). However, statistically, the gamma-band SFC (35 to 60 Hz) increased by a median of 10% with attention (106 increases, 77 decreases; $P < 0.02$). Delay-period firing rates were nonsignificantly increased by a median of 5% with attention (35 increases, 26 decreases; $P = 0.13$). During the stimulus period (Fig. 3, C and D), low-frequency SFC was reduced by a median of 23% with attention (142 decreases, 65 increases; $P < 10^{-6}$), whereas gamma-frequency SFC increased by a median of 19% (167 increases, 40 decreases; $P < 10^{-6}$). Firing rates were enhanced by a median of 16% with attention (68 increases, one decrease; $P < 10^{-6}$). Attention affected the normalized power spectrum of the raw LFP essentially in the same way as the SFC.

The above analysis of the sustained re-

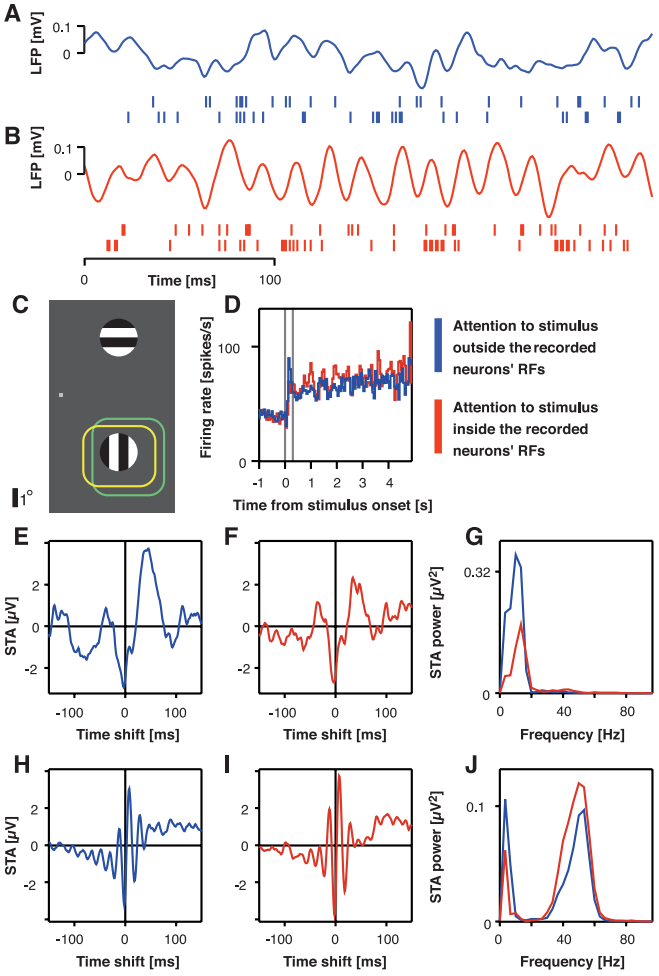

Fig. 1. Attentional modulation of oscillatory synchronization between spikes and LFP from two separate electrodes. Raw stimulus–driven LFP and multi-unit activity with attention outside the RF (**A**) and into the RF (**B**). (**C**) RFs (not visible to monkey; green: spike recording site, yellow: LFP recording site); fixation point and grating stimuli are to scale. The RFs for both recording sites were determined from the multi-unit activity and included only one of the two stimuli. In separate trials, this stimulus was either attended or ignored. Data are from 300 correct trials per attention condition. (**D**) Firing-rate histograms. Vertical lines indicate stimulus onset and 300 ms after stimulus onset. Delay period was the 1-s interval before stimulus onset, and stimulus period was from 300 ms after stimulus onset until one of the stimuli changed its color. Delay-period STAs for attention outside the RF (**E**) and into the RF (**F**) and the respective power spectra (**G**). Stimulus-period STAs for attention outside the RF (**H**) and into the RF (**I**) and the respective power spectra (**J**).

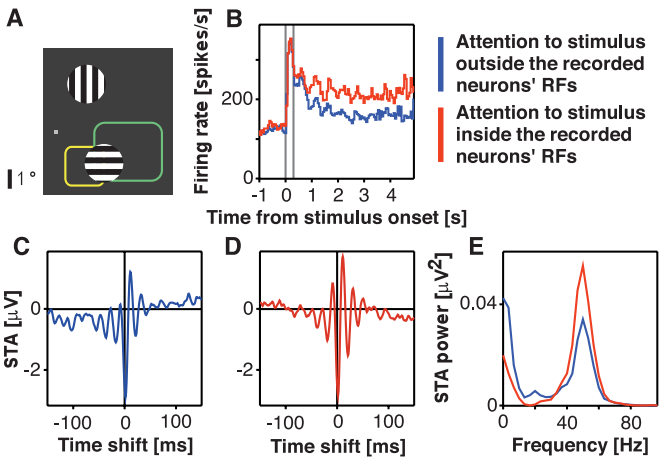

Fig. 2. Attentional modulation of synchronization has high spatial resolution in the cortex. Conventions are as for Fig. 1 except that the stimulus outside the RF is only 1.5° from the RF border. Spikes and LFP are from two separate electrodes. Data are from 125 correct trials per attention condition. (**A**) RFs, fixation point, and grating stimuli. (**B**) Firing-rate histograms. (**C** and **D**) STAs for stimulus period and (**E**) the respective power spectra.

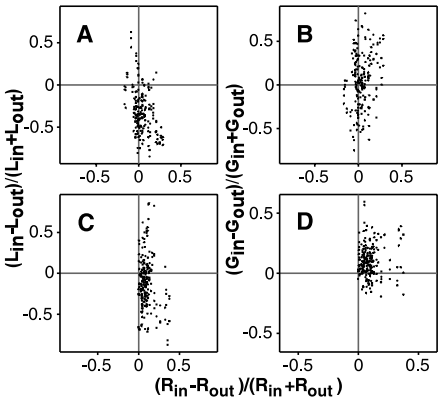

Fig. 3. Population measures of attentional effects on the SFC. Scatter plots compare attentional effects on low- and gamma-frequency SFC and on firing rates. Each dot represents one pair of recording sites. The *x*- and *y*-axis values are attentional indices defined as AI(P) = [P(in) − P(out)]/[P(in) + P(out)], with P being one of the three parameters under study: low-frequency synchronization (L), gamma-frequency synchronization (G), and firing rates (R). P(in) is the value of the parameter with attention directed into the RF, and P(out), with attention directed outside the RF. (**A** and **B**) Activity from the 1-s delay period before stimulus onset. (**C** and **D**) Activity from the stimulus period.

sponse excluded the first 300 ms after stimulus onset to avoid response-onset transients (*22*). We separately analyzed the poststimulus time course of firing rates and LFP. For the recording site shown as an example in Fig. 4B, attention did not affect the mean firing rate until about 420 ms after stimulus onset, consistent with other recent studies in which a single high-contrast stimulus in the RF was used (*26*, *27*). By contrast, synchronization was modulated by attention very early in the response. STAs for the 100-ms period after response onset (starting 50 ms after stimulus onset) contained large low-frequency modulations with superimposed gamma-frequency modulations (Fig. 4D). The low-frequency (10 Hz) synchronization was reduced by attention (Fig. 4E). Conversely, there was a smaller gamma-frequency peak at around 65 Hz that was enhanced by attention (Fig. 4, F and G). Both the visual evoked potential (VEP) (Fig. 4A) and the spike histogram (Fig. 4B) contained strong stimulus-locked gamma-frequency oscillations in the first 100 ms of the response (Fig. 4C). Thus, this very early gamma-frequency synchronization was at least partially locked to stimulus onset (*28*), whereas oscillatory synchronization during the later, sustained visual response was not stimulus locked.

Similar observations were made across the population. Attention did not modulate mean firing rates in the period from 50 to 150 ms after stimulus onset (median decrease, 0.5%; 32 decreases, 29 increases; $P = 0.35$), and significant sustained attentional effects on mean firing rate did not begin until about 450 ms (*29*). By contrast, low-frequency SFC in the 50- to 150-ms period was reduced by a median of 8% (108 decreases, 75 increases; $P < 0.01$) with attention, whereas gamma-frequency (40 to 90 Hz) synchronization was enhanced by a median of 16% (114 increases, 69 decreases; $P < 0.0005$). VEPs showed low-frequency power in the 50- to 150-ms period reduced by a median of 12% (45 decreases, 19 increases; $P < 0.001$) with attention, whereas gamma-frequency power was increased by a median of 19% (48 decreases, 16 increases; $P < 0.00005$). Spike histograms showed a median 15% increase in gamma-frequency power with attention (38 increases, 23 decreases; $P < 0.05$) but only a weak tendency for reduced low-frequency power (−2%; 33 decreases, 28 increases; $P = 0.26$).

In summary, attention increased gamma frequency and reduced low-frequency synchronization of V4 neurons representing the behaviorally relevant stimulus. This held true even during the delay period and in the first few hundred milliseconds after response onset, when firing rates were not affected. Gamma-frequency synchronization has been found in visual cortex in the absence of selective attention (*8*, *17*) and can be enhanced by brainstem stimulation (*30*), presumably via cholinergic pathways (*31*). However, the mechanisms that mediate the effects of selective visual attention presented here are not yet clear. Although attention increased gamma frequency and reduced low-frequency synchronization among the large majority of affected neurons, we did find cases with opposite effects. This raises the interesting possibility that attention actually sets a specific synchronization pattern among the affected neurons.

The observed changes in synchronization may enhance the impact of the affected neurons on postsynaptic targets. Gamma-frequency synchronization causes spikes to coincide within 10 ms (half the cycle length of ≈20 ms), enhancing their impact on postsynaptic neurons (*32*, *33*). Low-frequency desynchronization may also enhance postsynaptic efficacy by reducing spike co-occurrence within 50 to 100 ms, thereby avoiding spike-frequency adaptation effects with time constants of 15 to 50 ms (*34*). Spike-frequency adaptation does not affect spikes correlated at gamma frequencies, because these spikes coincide in a shorter interval than the adaptation time constant.

V4 output neurons project to the inferior temporal (IT) cortex. In the RF of IT neurons, attended stimuli have an advantage over competing distracters (*2*, *3*). Models that explain the competitive advantage of attended stimuli assume an enhanced efficacy of inputs from neurons at earlier stages activated by the attended stimulus (*6*, *10*). One possibility is that synchronized inputs from V4 cells responding to attended stimuli activate not only excitatory IT neurons but also interneurons, which in turn inhibit IT cells that receive inputs from distracters. A similar mechanism might be at work in V4 itself, if V2 inputs to V4 are also synchronized for attended stimuli. If competitive interactions between neurons in V4 were restricted to cells with overlapping RFs, this would explain why responses to distracters in the RF are typically not suppressed in V4 when the attended stimulus is far from the RF [(*2*, *5*, *7*); see, however, (*35*–*37*)]. With attention, synchronized outputs from V2 or V4 will likely synchronize the firing of postsynaptic neurons in V4 or IT, respectively, thereby enhancing the impact of these cells on subsequent stages of processing, even when mechanisms such as response saturation minimize changes in absolute firing rates (*26*).

An increased impact of a neuronal population on its postsynaptic targets is equivalent to an increase in effective synaptic gain. Previous studies have proposed an increase in synaptic gain to explain a wide variety of behavioral influences (*6*, *38*–*40*) on neuronal

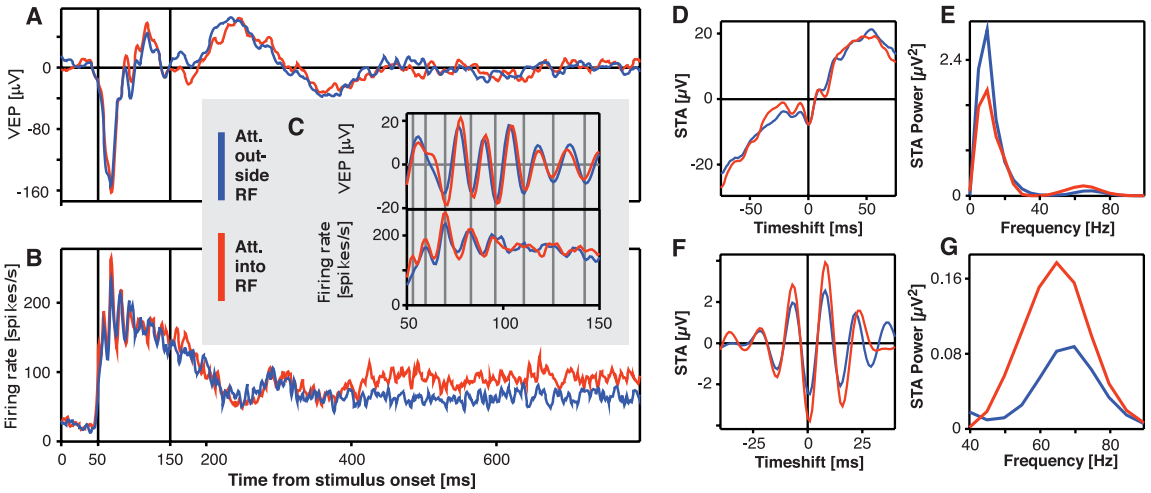

Fig. 4. Attention effects in early response. Data are from 300 correct trials per attention condition. VEPs (**A**) and spike histograms (**B**) from two separate electrodes as a function of time after stimulus onset. Vertical lines indicate the time period for which STAs (D and F) were calculated. The modulation of firing rate by attention starts only at about 420 ms after stimulus onset. From 50 to 150 ms after stimulus onset, there are stimulus-locked gamma-frequency oscillations in firing rate synchronized with LFP fluctuations. Gamma-frequency oscillations are shown in detail (**C**) with the LFP filtered (40 to 90 Hz) and vertical lines indicating peaks of the rhythmic population activity. (**D**) STAs for 50 to 150 ms after stimulus onset and (**E**) the respective power spectra. (**F**) The STA from (D), filtered (40 to 90 Hz), and (**G**) the respective part of the power spectrum.

firing rates. Increasing the effective synaptic gain by modulating synchronization at precise locations in the cortex might therefore be a fundamental neuronal mechanism for amplifying signals that represent behaviorally relevant stimuli.

References and Notes

1. R. Desimone, J. Duncan, *Annu. Rev. Neurosci.* **18**, 193 (1995).
2. J. Moran, R. Desimone *Science* **229**, 782 (1985).
3. L. Chelazzi, E. K. Miller, J. Duncan, R. Desimone, *Nature* **363**, 345 (1993).
4. S. Treue, J. H. Maunsell, *Nature* **382**, 539 (1996).
5. S. J. Luck, L. Chelazzi, S. A. Hillyard, R. Desimone, *J. Neurophysiol.* **77**, 24 (1997).
6. J. H. Reynolds, L. Chelazzi, R. Desimone, *J. Neurosci.* **19**, 1736 (1999).
7. B. C. Motter, *J. Neurophysiol.* **70**, 909 (1993).
8. C. M. Gray, P. König, A. K. Engel, W. Singer, *Nature* **338**, 334 (1989).
9. F. Crick, C. Koch, *Semin. Neurosci.* **2**, 263 (1990).
10. E. Niebur, C. Koch, C. Rosin, *Vision Res.* **33**, 2789 (1993).
11. V. N. Murthy, E. E. Fetz, *J. Neurophysiol.* **76**, 3968 (1996).
12. S. Makeig, T. P. Jung, *Brain Res. Cogn. Brain Res.* **4**, 15 (1996).
13. P. R. Roelfsema, A. K. Engel, P. König, W. Singer, *Nature* **385**, 157 (1997).
14. P. Fries, P. R. Roelfsema, A. K. Engel, P. König, W. Singer, *Proc. Natl. Acad. Sci. U.S.A.* **94**, 12699 (1997).
15. J. P. Donoghue, J. N. Sanes, N. G. Hatsopoulos, G. Gaal, *J. Neurophysiol.* **79**, 159 (1998).
16. T. Gruber, M. M. Müller, A. Keil, T. Elbert, *Clin. Neurophysiol.* **110**, 2074 (1999).
17. P. E. Maldonado, S. Friedman-Hill, C. M. Gray, *Cereb. Cortex* **10**, 1117 (2000).
18. E. Salinas, T. J. Sejnowski, *J. Neurosci.* **20**, 6193 (2000).
19. P. N. Steinmetz *et al.*, *Nature* **404**, 187 (2000).
20. Animal care was in accordance with NIH guidelines. Standard procedures were used to record spike and LFP activity simultaneously from four extracellular electrodes in V4 of two monkeys (electrode separations of 650 or 900 μm; Plexon data acquisition system). The LFP (filtered at 1 to 100 Hz) reflects the average transmembrane currents of neurons in a volume of a few hundred micrometers radius around the electrode tip (*41*). Negative values of LFP correspond to neuronal activation. Spike waveforms were stored for offline sorting. We pooled all neurons recorded through a given electrode [≈2 to 10 neurons; see supplementary information (*24*)]. The resulting multi-unit almost always showed clear oscillatory synchronization. Analysis of single units revealed that some showed much stronger oscillatory synchronization than others. Whenever there was clear oscillatory synchronization, attention effects were essentially identical, irrespective of whether the spikes were pooled or from an isolated neuron.
21. The cue directing attention was either a short (0.75°) line next to the fixation spot, pointing to the location of the target, or the fixation spot color, with red cueing the upper stimulus and green, the lower stimulus. The delay between cue and stimulus onset was 1500 to 2000 ms, and the cue remained throughout the trial. In a subset of recordings, we used a blocked trial design without any explicit cue. All paradigms gave essentially the same results. Stimuli were pure luminance gratings (100% contrast, 2° to 3° diameter, 1° to 2°/s drift rate, one to two cycles per degree of spatial frequency) with a frame rate of 120 Hz. The grating inside the RF had the optimal orientation to coactivate cells at as many of the electrodes as possible. The grating outside the RF was always in another quadrant and orthogonal to the inside RF grating, and did not activate the recorded neurons. After a random interval of 500 to 5000 ms, the white stripes of the cued (target) stimulus changed to isoluminant yellow. The color change was close to the monkey's detection threshold, ensuring that the task could be performed only when attention was focused on the target. The monkey was rewarded if it maintained fixation throughout the trial and released a bar within 650 ms of the color change. In half of the trials, the same color change occurred for the uncued (distracter) stimulus. Responses to distracter changes resulted in a time-out without reward. Performance was 83 to 87% correct. We recorded 100 to 300 correct trials per attention condition. Eye position for the two attention conditions differed by 16 arcmin (delay) to 13 arcmin (stimulus period).
22. We calculated STAs by averaging all LFP segments at ±150 ms around all spikes recorded under one attentional condition. Only STAs of LFPs and spikes recorded from separate electrodes were used in the analyses. However, STAs of LFPs and spikes recorded on a single electrode showed essentially identical effects. For the analysis of the sustained response, the 300 ms after stimulus onset was discarded because it always contained stimulus-locked modulations in the LFP. Thereafter, stimulus-locked components were largely absent and shift-predictor STAs flat. For direct comparisons between sustained response synchronization and firing rates, only spikes used for STA compilation were used. We also calculated cycle-triggered averages (CTAs) of spike times (*11*) by band-pass filtering the LFP in a predefined range and triggering the spike-time averaging by troughs in the filtered LFP. After normalization for average spike rate, CTAs give changes in firing rate around cycle triggers. The CTAs showed qualitatively the same attention effects as STAs. Cross-correlation histograms (CCHs) of spike times proved much less sensitive than STAs in detecting oscillatory synchronization. STAs often revealed oscillatory synchronization where CCHs did not. See supplementary information (*24*) for a comparison of the different measures.
23. M. S. Worden, J. J. Foxe, N. Wang, G.V. Simpson, *J. Neurosci.* (Online) **20**, RC63 (2000).
24. Supplementary data are available on *Science* Online at www.sciencemag.org/cgi/content/full/291/5508/1560/DC1.
25. For statistical analysis, we used the frequency bands that were obvious from the SFC spectra. Results remain essentially unchanged for small variations (±6.7 Hz). Unless stated otherwise, we used a paired Sign test.
26. J. H. Reynolds, T. Pasternak, R. Desimone, *Neuron* **26**, 703 (2000).
27. S. Treue, D. R. Patzwahl, paper presented at the 30th Annual Meeting of the Society for Neuroscience, New Orleans, LA, 6 November 2000.
28. Cross-correlations between monitor refreshes and either spikes or LFP showed no sign of locking. Thus, early gamma-frequency synchronization was locked to stimulus onset but not to stimulus flicker.
29. We compared firing rates (1-ms bin width) for the two attentional conditions across all recording sites using a paired t test. The first five consecutive significant ($P < 0.05$) bins defined the onset of consistent attentional modulation.
30. M. H. Munk, P. R. Roelfsema, P. König, A. K. Engel, W. Singer, *Science* **272**, 271 (1996).
31. E. H. Buhl, G. Tamas, A. Fisahn, *J. Physiol.* **513** 117 (1998).
32. J. M. Alonso, W. M. Usrey, R. C. Reid, *Nature* **383**, 815 (1996).
33. R, Azouz, C. M. Gray, *Proc. Natl. Acad. Sci. U.S.A.* **97**, 8110 (2000).
34. B. Ahmed, J. C. Anderson, R. J. Douglas, K. A. Martin, D. Whitteridge, *Cereb. Cortex* **8**, 462 (1998).
35. H. Spitzer, R. Desimone, J. Moran, *Science* **240**, 338 (1988).
36. C. E. Connor, J. L. Gallant, D. C. Preddie, D. C. Van Essen, *J. Neurophysiol.* **75**, 1306 (1996).
37. C. J. McAdams, J. H. R. Maunsell, *J. Neurosci.* **19**, 431 (1999).
38. R. A. Andersen, G. K. Essick, R. M. Siegel, *Science* **230**, 456 (1985).
39. B. A. Olshausen, C. H. Anderson, D. C. Van Essen, *J. Neurosci.* **13**, 4700 (1993).
40. E. Salinas, L. F. Abbott, *Proc. Natl. Acad. Sci. U.S.A.* **93**, 11956 (1996).
41. J. D. Frost Jr., *Electroencephalogr. Clin. Neurophysiol.* **23**, 89 (1967).

42. We thank Plexon Incorporated for technical assistance, A. Rossi for help during the experiments, and F. Crick, C. Gray, and C. Koch for valuable comments on the manuscript.

5 September 2000; accepted 22 December 2000

Modulation of Oscillatory Neuronal Synchronization by Selective Visual Attention

Pascal Fries, John H. Reynolds, Alan E. Rorie, and Robert Desimone

Supplementary Material

1.) The multi-unit signal:

During recording sessions, we stored all putative spike waveforms (Web fig. 1 for a representative example recording session). Offline, we rejected waveforms corresponding to late parts of multi-phasic spikes and, in a few cases, electrical or movements artifacts due to licking etc.. We used principal component analysis to sort waveforms from different single cells (Web fig. 1A). Clusters that clearly separated from the origin of the PCA plot and from other clusters were considered single units. There was usually one cluster close to the origin with low-amplitude waveforms that could not be clearly differentiated into separate single units. The multi-unit signal used in all of our analyses was pooled from the isolated single units and the non-differentiated cluster of units. This multi-unit signal showed the most reliable oscillatory synchronization. We also analyzed the single units separately and found that whereas some of them showed very strong oscillatory synchronization, many showed little or no synchronization. Whenever there was clear oscillatory synchronization, attention diminished low frequency and enhanced gamma frequency synchronization, irrespective of whether the spikes were from the pooled multi-unit signal or were from an isolated neuron.

Supplemental Figure 1. (**A**) Each dot in this scatter plot corresponds to the waveform of one spike from one recording site, giving the coefficient of the first principal component on the X-Axis and the coefficient of the second principal component on the Y-Axis (scale not shown). Dots colored in blue had been identified as late parts of a multi-phasic spike and were eliminated. The remaining dots, shown in yellow, form three distinct clusters. Fifty example waveforms from each cluster are shown in (**B**). We classified the waveforms shown in red and blue as single units and the ones shown in gray as non-differentiated units.

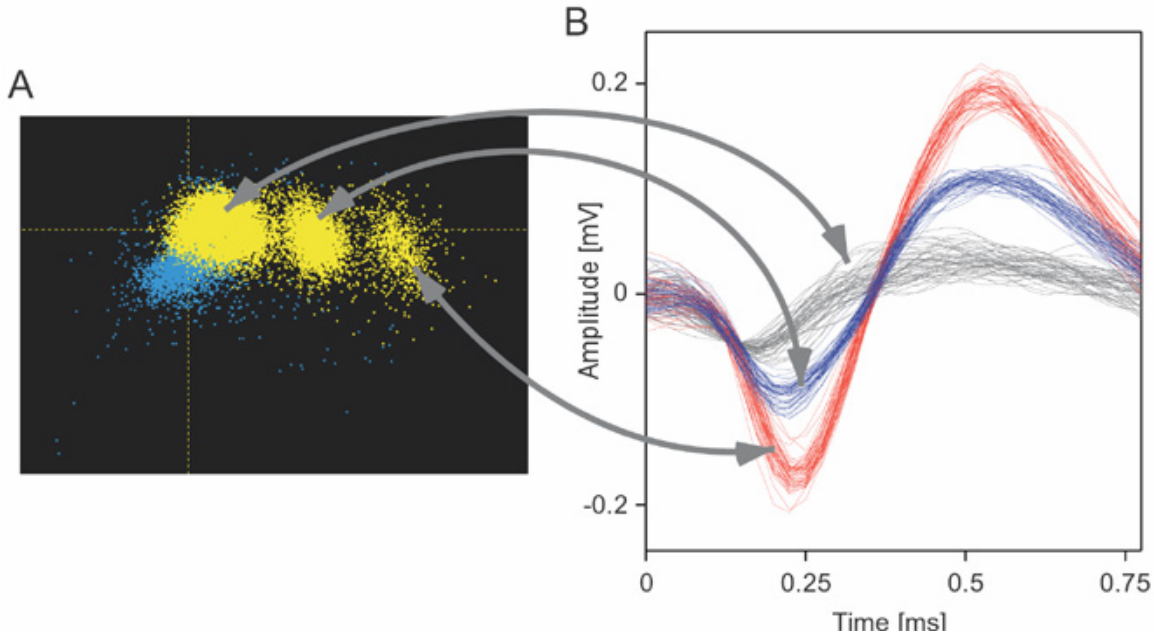

2.) High sensitivity of the STA in detecting local neuronal synchronization:
In order to measure local neuronal synchronization, we used the spike-triggered average of the LFP (STA). If spike times have a reliable temporal relation to the local neuronal activity as measured by the LFP, then LFP fluctuations add up during the spike triggered averaging process. On the other hand, if spike times have no temporal relation to the activity of surrounding neurons, fluctuations in the LFP average out during STA compilation, resulting in a flat STA. The STA is very sensitive in detecting synchronization because the LFP averages over many neurons. However, the STA possesses all the selectivity that is typical for spike responses, because without spikes or with spikes that have no temporal relation to the LFP fluctuations, the STA is flat.

We also calculated cross-correlation histograms (CCHs) for all pairs of spike recordings. In contrast to STAs, CCHs rarely exhibited modulations, and, if present, they were of small amplitude. The discrepancy between the STA and the CCH is due at least in part to the fact that the STA uses the LFP, which is a reliable measure of the population activity with millisecond resolution. For example, we found that two spike trains can show strong locking to one LFP, but at the same time only weak synchronization with respect to each other. An example of this is given in Web figure 2. Finally, it is clear that only a subpopulation of individual neurons participates in synchronization.

Supplemental Figure 2. (**A**) A 400 ms segment of LFP from one recording site (Elec 1) and two simultaneously recorded spike trains from two different recording sites (Elec 2 and Elec 3). The LFP shows clear gamma-frequency fluctuations and some spikes seem to be locked to the LFP negativities. (**B**) STA calculated with the spikes from Elec 2 and the LFP from Elec 1. The graph shows the STA as black line and the STA±2SEM as gray shaded band. (**C**) shows the same analysis as (**B**) but with spikes from Elec 3. Both STAs show clear spike-field synchronization with a high signal to noise ratio as can be judged from the width of the gray shaded band. (**D**) shows the cross-correlation histogram of

spikes recorded from Elec 2, normalized for the number of trigger spikes from Elec 3. Note that the y-axis is truncated to allow comparison with the STAs. The CCH shows less modulation and a much lower signal to noise ratio than the STAs. For this example, we picked one of the most strongly modulated CCHs from our sample of CCHs, while the STAs are fairly representative for the whole sample of STAs. Many CCHs do not show any sign of oscillatory synchronization, while almost all STAs do.

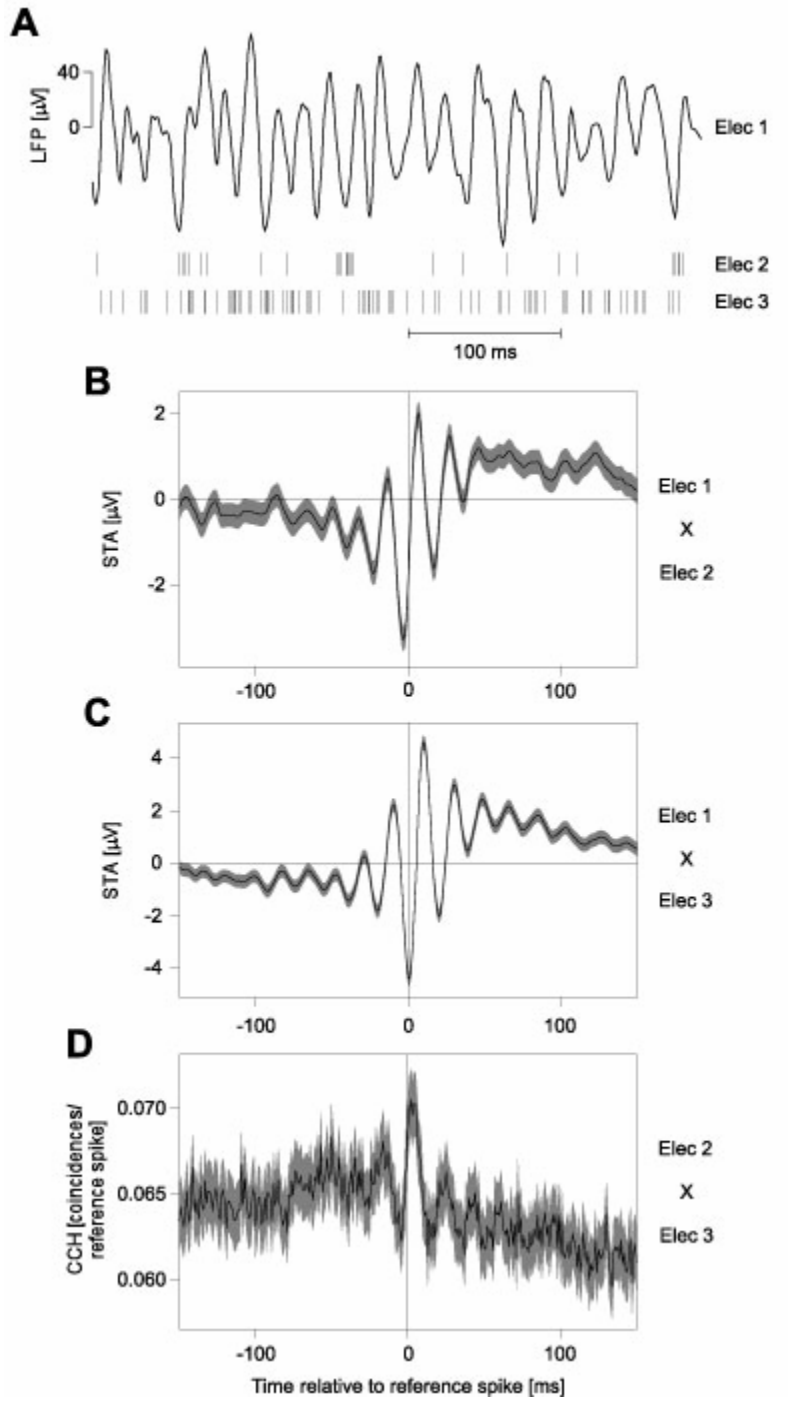

3.) Calculation and interpretation of the spike-field coherence:
The spike-field coherence (SFC) measures phase synchronization between the local field potential (LFP) and spike times as a function of frequency. For the calculation of the SFC, we first obtain for each spike the LFP segment for a short time window around that spike (typically ±100 ms or ±150 ms). Averaging these LFP segments gives the spike-triggered average (STA). Any components of the LFP that are not consistently phase locked to the spikes are averaged out and are not visible in the STA. As the STA is calculated by summing all LFP segments and then dividing by the number of spikes, the STA is normalized for spike number. In order to quantify the STA, we calculate its (absolute) power spectrum. The power spectrum gives the magnitude of all frequency components of the STA as a function of frequency. The power spectrum of the STA is still dependent on the power spectrum of the LFP itself. Multiplying the LFP by a factor F would magnify the STA by that factor and would therefore magnify its power by 0.5*F2, despite the absence of any change in the phase synchronization between spikes and LFP. In order to quantify the phase synchronization between spikes and the LFP, it is therefore necessary to normalize the power spectrum of the STA. We normalize the power spectrum of the STA by the average of all power spectra of all LFP segments that were averaged to obtain the STA. This normalization gives the SFC, which is independent of the firing rate of the spikes and of the power spectrum of the LFP. If the SFC for any given frequency is 1, then this means that all spikes appear at exactly the same phase relation relative to this frequency component. If the SFC for any given frequency is 0, then this means that the spikes do not have any systematic phase relation to the LFP component at this frequency. We illustrate the calculation and interpretation of the SFC in Web figs. 3 and 4.

Supplemental Figure 3. The spike field coherence. In this figure, we use artificially constructed data to demonstrate how the spike field coherence is calculated and to indicate how it should be interpreted. (**A**) and (**B**) show two components which constitute a signal (**C**) that we use here as a hypothetical LFP. The high amplitude component shown in (**A**) has a frequency of 10 Hz, while the low amplitude signal in (**B**) has a frequency of 50 Hz. Note that for the purposes of this figure, we have chosen a signal that contains power in only two frequency bins. In a real LFP, the spectral power is typically concentrated in frequency bands, not in single frequency bins of the spectrum. The vertical lines in panels (**A**) through (**C**) mark hypothetical spike times, which are the same for all three panels. The spikes are exactly locked to the negativities of the 50 Hz component and occur in a random subset of the 50 Hz periods. The spikes have no phase relation to the 10 Hz component. (**D**) and (**E**) show two examples of segments of the artificial LFP from the period around (±100 ms) two spike occurrences. The power spectra of these LFP pieces are shown in (**F**) and (**G**), respectively. The 10 Hz component with the amplitude of 1 mV has a power of 0.5*(1 mV)2 = 0.5 mV2 and the 50 Hz component with the amplitude of 0.2 mV has a power of 0.02 mV2, respectively. Note that the two spikes occur at different times during the phase of the 10 Hz oscillation, but this phase information is not represented in the power spectrum. (**H**) shows the average of the LFP segments around (±100 ms) all 15 spikes. This average is called the spike-triggered average or STA. As the spikes are perfectly phase locked to the 50 Hz component, this component has the same amplitude in the STA as it had in the original

signal, namely 0.2 mV. However, the spikes have no phase relation to the 10 Hz component and therefore, the amplitude of this component is strongly reduced in the STA as compared to its amplitude in the original artificial LFP signal. This is true even for the small number of 15 spikes used in this exmple. With increasing numbers of spikes, the 10 Hz component of the STA would quickly disappear completely. This differential reduction in power can be seen in the power spectrum of the STA, that is shown in (**I**). The power at 50 Hz is 0.02 mV2 just as it was in the original signal, but the power at 10 Hz is only 0.008 mV2, which is only 1.6% of the original 0.5 mV2. (**J**) shows the average of all power spectra of all the 15 LFP pieces (surrounding the 15 spikes) that were averaged to give the STA. This average power spectrum looks exactly like the power spectra (**F**) and (**G**) for the two examples of LFP segments in (**D**) and (**E**). Thus, it contains much more power at 10 Hz than at 50 Hz. Dividing (**I**) by (**J**) gives the spike-field coherence or SFC, which is shown in (**K**). Note, that the SFC is not a power measure, but a unitless measure that assumes the value one for perfect phase synchronization and the value zero for no phase synchronization. The SFC for these artificial data shows that the spikes are perfectly locked to the 50 Hz component. At 10 Hz, the SFC also shows some phase synchronization, which is due to the low number of spikes, resulting in insufficient averaging. With increasing numbers of spikes, the SFC at 10 Hz would quickly approximate zero

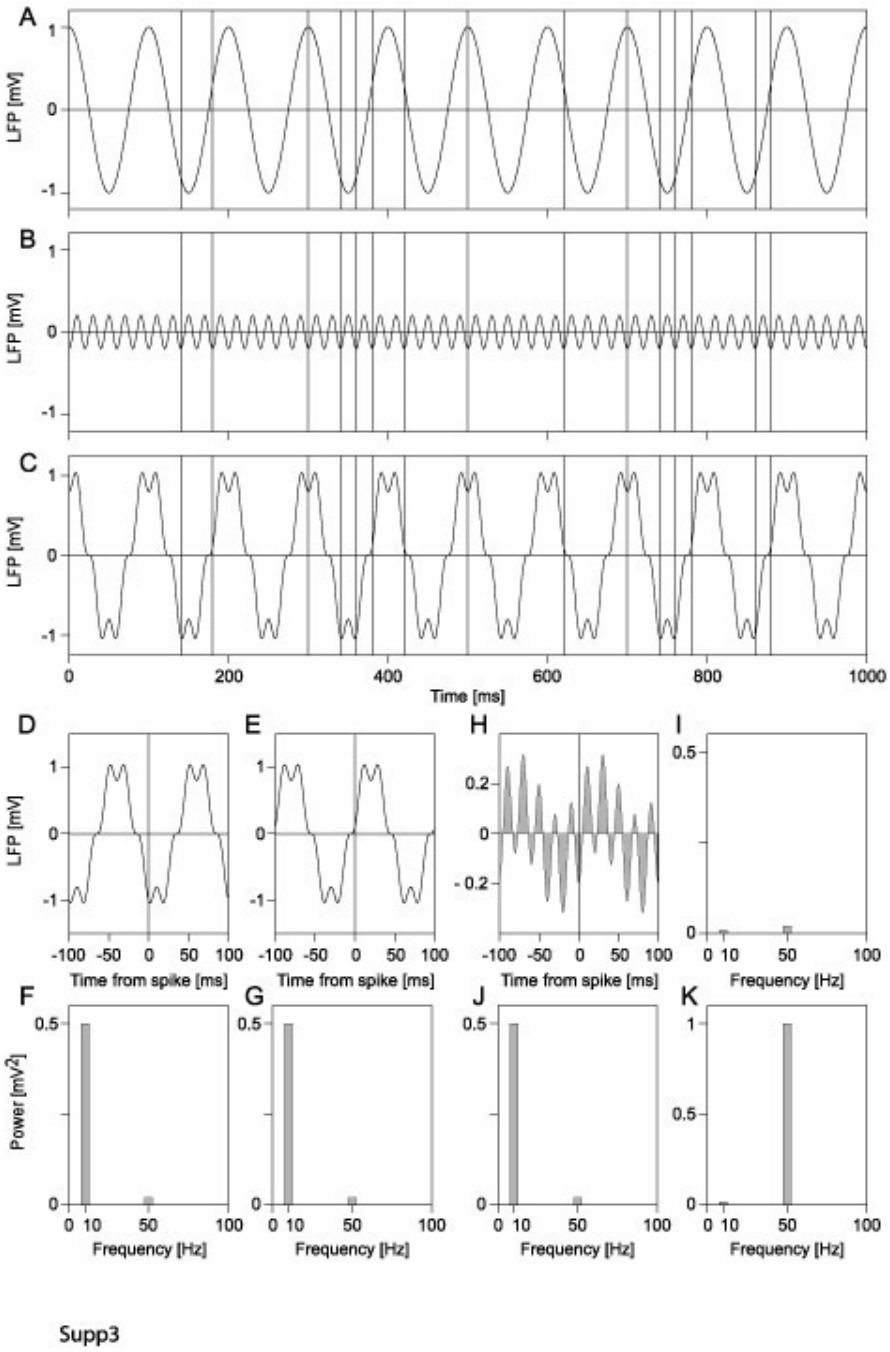

Supp3

Note that the 10 and the 50 Hz component of the LFP have a fixed phase relation. But the spikes are only phase locked to the 50 Hz component. The SFC shows this selective synchronization of the spikes to the 50 Hz component. In addition, the SFC ignores the higher amplitude of the 10 Hz component in the LFP, because it is normalized by the average of all power spectra (**J**).

Supplemental Figure 4. In this figure, we repeat the analysis from Web fig. 3, however, this time only half of the spikes are phase locked to the 50 Hz LFP oscillation, while the other half of the spikes occur at random times. Note that the SFC shown in (**K**) is now 0.5

for the 50 Hz bin. This reflects the fact that only 50 percent of the spikes are locked to the 50 Hz oscillation. The 10 Hz SFC is further reduced as compared to Web fig. 3, because the 10 Hz oscillation is averaged out more completely, by the larger number of spikes. [Note: A correction has been made to this figure. See below.]

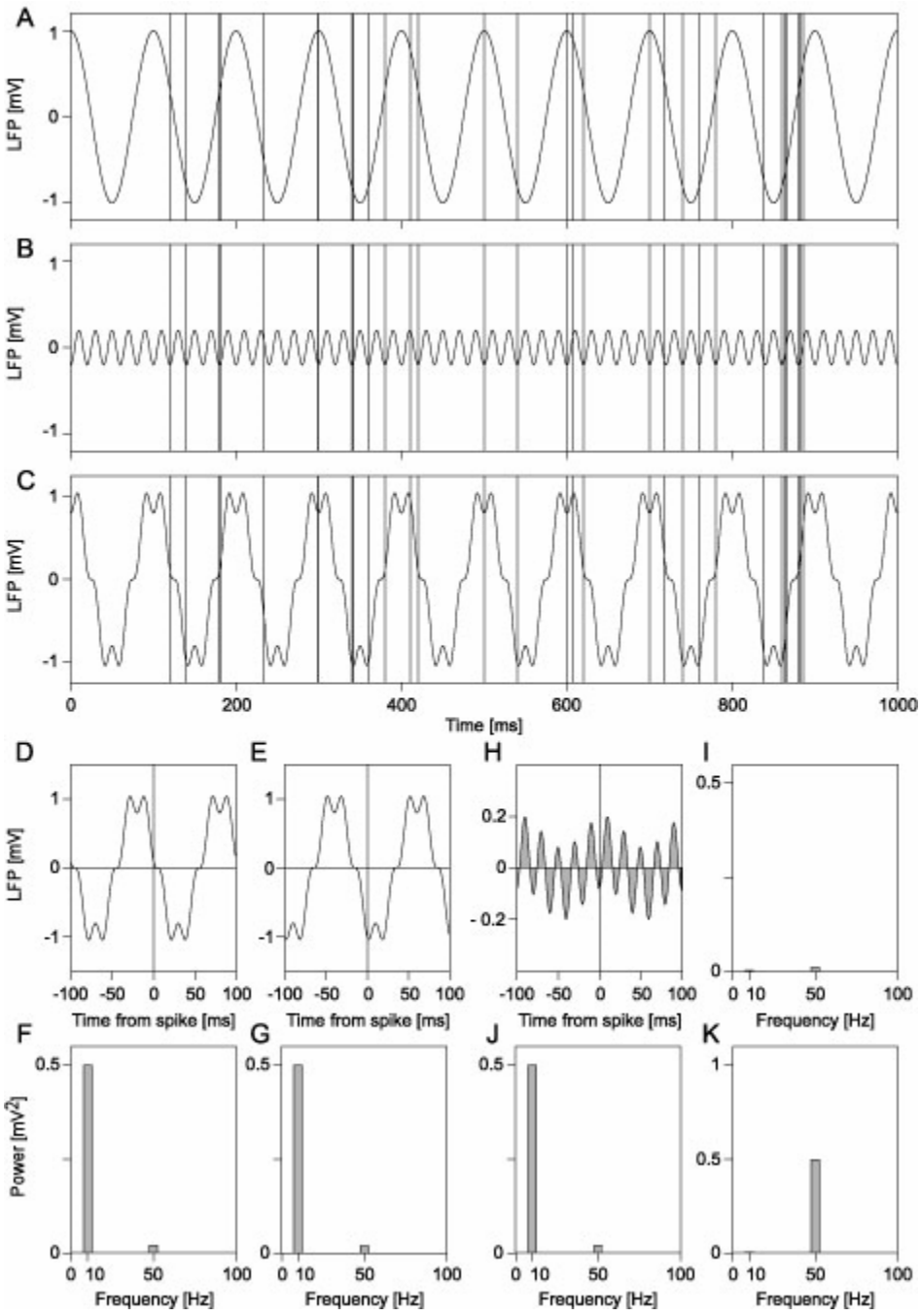

Medium version | Full size version

Correction to supplemental figures 3 and 4 (2 May 2003): Owing to a production error, supplemental figures 3 and 4 were swapped for one another in the original version of this supporting online material. The figures are correct in the current version. *Science* regrets the error.